脈衝雷射以特定功率密度於水溶液、大氣與真空環境下剝蝕多晶鈦靶之微結構及相變態研究

[1]黃俊傑、*[2]黃常寧

[1]中山大學材料與光電科學學系、[2]南臺科技大學化學工程與材料工程系

*cnhuang@stust.edu.tw

摘要

以光學顯微鏡與電子顯微鏡觀察脈衝雷射單一脈衝剝蝕多晶鈦靶，在靶材表面可得剝蝕坑與熱影響區，而其大小取決於雷射之能量密度與剝蝕過程所屬環境。 在不同剝蝕環境而相同雷射聚焦長度與功率密度下，剝蝕坑直徑變小而熱影響區寬度變大，其程度依序為水溶液、空氣與真空環境。在高功率雷射密度下剝蝕坑直徑變大於水溶液與空氣剝蝕環境，真空則維持不變，歸因於在此環境下具最小之雷射光寬化效應；熱影響區變大於真空與大氣剝蝕環境，水溶液則維持不變，則歸因於此環境下有效之熱消散效應。由電子繞射觀察於水溶液中雷射剝蝕鈦靶之橫截面，發現試片表面具較小之晶格間距，以 Birch-Murnagham 方程式計算其殘留應力達 17 GPa。在掃描式與穿透式電子顯微鏡觀察熱影響區呈現凝固與再結晶之組織，且形成次微米之 Ti_6O 與 Ti_3O 顆粒，這是由於在動態雷射剝蝕過程中高溫氧化所造成。

關鍵詞: 脈衝雷射剝蝕、熱影響區、聚焦離子束、再結晶組織、Birch-Murnagham 方程式、電漿引發壓力

Microstructure and Phase Changes of Polycrystalline α-Ti by Pulse Laser Ablation in Water, Air and Vacuum under Specified Power Density

[1]Jun-Jie Huang, *[2]Chang-Ning Huang

[1]Department of Materials and Optoelectronic Science, National Sun Yat-Sen University

[2]Department of Chemical and Materials Engineering, Southern Taiwan University of Science and Technology

Abstract

Polycrystalline α-Ti plates subjected to pulse laser ablation in a single pulse of specified energies showed crater and heat affected zone (HAZ) whose dimensions depend on the adopted power density and environment according to optical and electron microscopic observations. The crater diameter decreases, whereas HAZ width increases, in the order of water, air and vacuum environment under the same laser focal length and power density. A relatively high power density causes a significant increase of crater diameter for PLA in air and water but not vacuum with the least beam broadening effect. The increase of HAZ width with power density is significant for PLA in vacuum and air but not in water because of its effective heat dissipation. Electron diffraction of the cross sectioned α-Ti plates subjected to PLA in water showed smaller d-spacings in the upper level of the HAZ indicating a residual compressive stress up to ca. 17 GPa. The HAZ also showed solidified/recrystallized textures and submicron-sized Ti_6O and Ti_3O particles due to high temperature oxidation in the dynamic process.

Keywords: Pulsed Laser Ablation, Heat Affected Zone, Focused Ion Beam, Recrystallized Textures, Birch-Murnagham Equation, Plasma-induced Pressure

Received: Dec. 18, 2015; first revised: Feb. 22, 2016; accepted: March, 2016.

Corresponding author: C. -N. Huang, Department of Chemical and Materials Engineering, Southern Taiwan University of Science and Technology, Tainan, Taiwan.

I. Introduction

The motivation of this research is to compare the microstructure and phase changes of polycrystalline α-titanium (hcp) plate subjected to pulsed laser ablation (PLA) at specified conditions of pulse energy and the environment of water, air and vacuum. Laser processing under water has been widely used in steam cleaning, shock processing, welding, pulsed laser deposition and chemical surface modification. In general, laser ablation in water has better results in carrying debris, more effective cooling, increasing plasma pressure and higher optical breakdown threshold comparing with processing in air [1, 2].

Regardless of being processed in water, air or even vacuum, the laser-matter interaction during PLA depends strongly on the pulse duration, from nanosecond (ns) to femtosecond (fs), according to theoretical models and experimental results [3-5]. For example, during hole drilling or cutting of aluminum material, the thermal effects due to heat diffusion process typically produce a heat affected zone (HAZ) near the area irradiated by the laser beam for nanoseconds, but not fs [5]. The evolution of grain size in HAZ of aluminum material within nanoseconds was characterized by transmission electron microscopy (TEM) [5]. PLA on solids was also known to cause complicated phase transformations such as melting-solidification, sublimation-condensation and the formation of metastable phases, in particular the high-pressure phases due to very rapid heating and cooling of the nanosize condensates [6,7]. This has been proved experimentally by PLA on Ti target in air to fabricate α-PbO_2-type TiO_2 [6] and fluorite-type TiO_2 [7] nanocondensates with significant residual stress and fault/twinning associated with martensitic-type transformation according to TEM characterization. The high-pressure phase also occurs in the target subjected to PLA. For example, the silica window damaged by Nd:YAG laser (λ=355nm) with a 8.4 ns pulse width at a 10 Hz repetition rate in air showed a specific high-pressure silica phase, i.e. stishovite, according to electron diffraction and infrared reflectance measurements [8].

In this work, we focused on the combined effects of pulse energy/power density and environment, i.e. water, air and vacuum, on the width of the crater and HAZ in α-titanium plate under the same laser focal length when subjected to PLA in a single shot. For the sake of industrial importance, the ablated plate with the largest crater diameter yet least HAZ by PLA in water under a specified power density was used for detailed electron microscopic studies of defect microstructures, residual stress, as well as the extent of recrystallization and oxidation around the crater and HAZ.

II. Experimental

Polycrystalline α-Ti plate (99.95% pure, 10×10×1 mm^3) polished by diamond paste and then cleaned with ethanol was subjected to energetic Nd-YAG-laser (Lotis, 1064 nm in wavelength, beam mode: TEM00) pulse irradiation in water, air or vacuum ($3.5x10^{-5}$ torr) under Q-switch mode and laser parameters specified in Table 1. For the case of PLA in water, the target plate was put in a glass beaker filled with a fixed amount of DI water so that the target was 2 mm below the water level for laser focusing. The same focal length (i.e. the same beam diameter on the target) was used for PLA in water, air and vacuum under a specified power density, ranging from 9 to 11×10^{11} W/cm^2 depending on the pulse energy under a fixed pulse time duration of 16 ns in a single-pulse mode.

Optical microscopy coupled with Optimas 6.1 software was used to estimate the mean diameter of the hole and width of the HAZ exposed in the top-view image of the target plate. Scanning electron microscopy (SEM, JEOL JSM-6700F, 10 kV) was used to observe further details of the morphology and microstructures, in particular the grain size of the ablated surface.

Table 1 Experimental parameters for single-shot PLA on α-Ti under Q-switch mode

sample number	1	2	3	4
pulse energy (mJ/pulse)	430	470	500	520
pulse duration (ns)	16	16	16	16
beam size (mm^2)	0.03	0.03	0.03	0.03
fluence (J/cm^2)	1433	1567	1667	1733
frequency (Hz)	10	10	10	10
power density (10^{11} W/cm^2)	8.96	9.79	10.42	10.83

Focused Ion Beam (FIB, SII NanoTechnology Inc. SMI 3050) was used to make 1 micron thick sections for TEM studies across the crater, HAZ and the intact area of the target plates subjected to specific PLA treatments. The composition and crystal structures around the crater center and within the HAZ were characterized by analytical electron microscopy (AEM, JEOL 3010 instrument at 200 kV) with selected area electron diffraction (SAED), and point-count energy dispersive X-ray (EDX) analysis at a beam size of 1 nm. Point-count EDX analysis of local areas of interest was performed using K shell counts for Ti and O, and the principle of ratio method without absorption correction [9]. Bright field images (BFIs) taken by TEM were used to study the general morphology and grain size around the hole and within the HAZ. The d-spacings measured from SAED patterns taken with a selected area aperture of 1 μm were used for least-squares refinement of the lattice parameters for the residual stress estimation of the ablated α-Ti plate based on the ambient cell parameters reported in JCPDS file #44-1294 and Birch-Murnagham equation of state having the isothermal bulk modulus B = 117 GPa and its pressure derivative B'= 3.9 GPa for bulk α-Ti [10].

III. Results

1. Metallographic observations of PLA induced microstructures

The α-titanium plates all formed a single crater with surrounding HAZ when subjected to different laser pulse energy and environment. The crater diameter turned out to be decreasing whereas HAZ width increasing in the order of water, air and vacuum environment under the same focal length and power density. Figs. 1a, 1b and 1c show the representative top-view optical micrograph of such features produced by the specified pulse energy 520 mJ/pulse in water, vacuum and air, respectively. It is noteworthy that the smallest crater has a central hole throughout the target plate in the case of Fig. 1c.

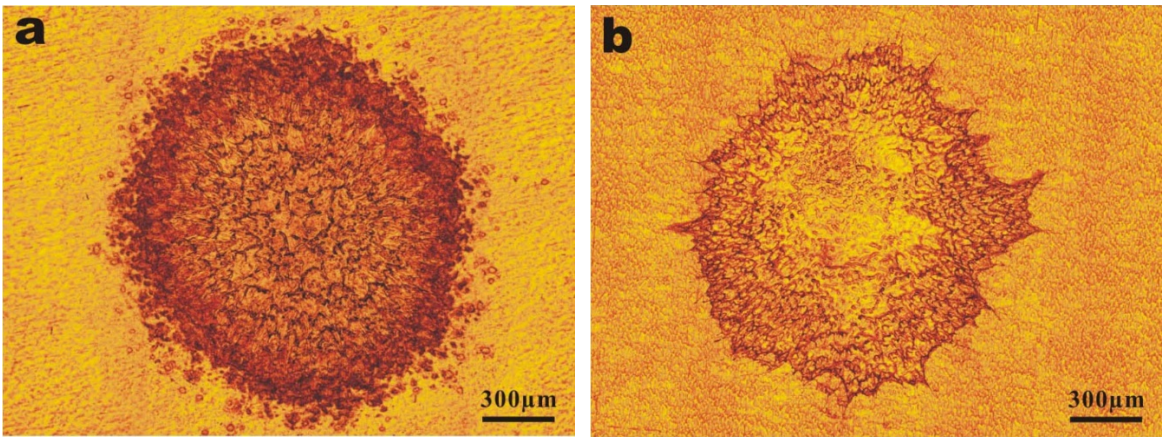

(a)water (b)air

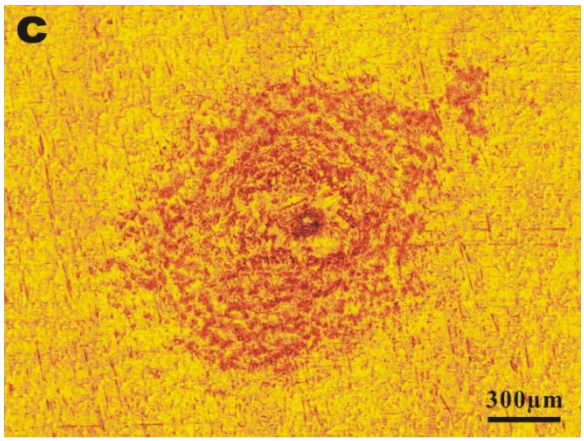

(c) vacuum

Fig. 1 Optical micrographs under reflective light of the α-titanium plates showing top view of their craters and surrounding HAZs formed by PLA at 520 mJ/pulse under single-shot Q-switch mode.

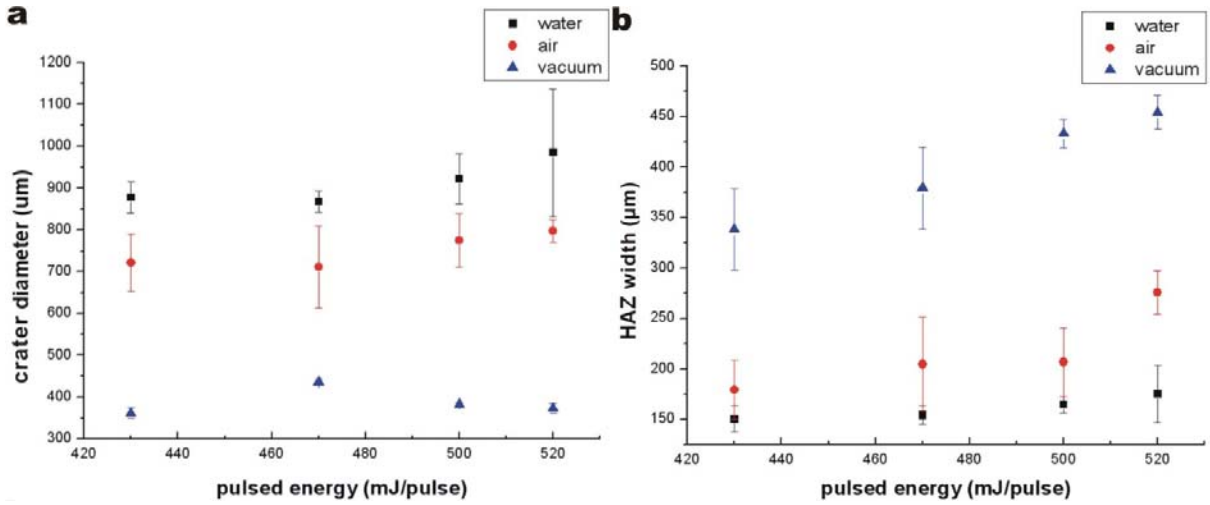

(a) crater diameter (b) HAZ width

Fig. 2 Pulse energy dependence of crater diameter and HAZ width in α-Ti plate subjected to PLA in water (squares), air (circles) and vacuum (triangles) using single-shot Q-switch mode.

The crater diameter and HAZ width as a function of pulse energy are further compiled in Figs. 2a and 2b, respectively. Apparently, relatively high pulse energy causes a slight increase of crater diameter when produced in air and water, but no significant change when produced in vacuum (Fig. 2a). By contrast, higher pulse energy caused a significant increase of HAZ width when produced in vacuum and air but not in water (Fig. 2b).

SEM observations indicated that the ablated Ti plate has varied extent of melting, cracking and porosity near the crater regardless of the pulse energy and environments adopted. Fig. 3 shows the representative top view of surface microstructures produced by PLA in water at 520 mJ/pulse. The SEM secondary electron images taken at low and high magnifications from three areas, i.e. (a) near the crater center, (b) between the crater center and HAZ and (c) within the HAZ, showed progressively lesser extent of melting, cracking and porosity. There is most extensive melting with curved solidification front more or less overlaid with the condensation particles when subject to pulse energy concentration near the crater center (Fig. 3a). Round cracks and pits, presumably due to thermal stress and thermal etching, are typical to the area between the crater center and HAZ (Fig. 3b), whereas dendritic solidification front, due to considerable extent of supercooling, is typical to HAZ (Fig. 3c).

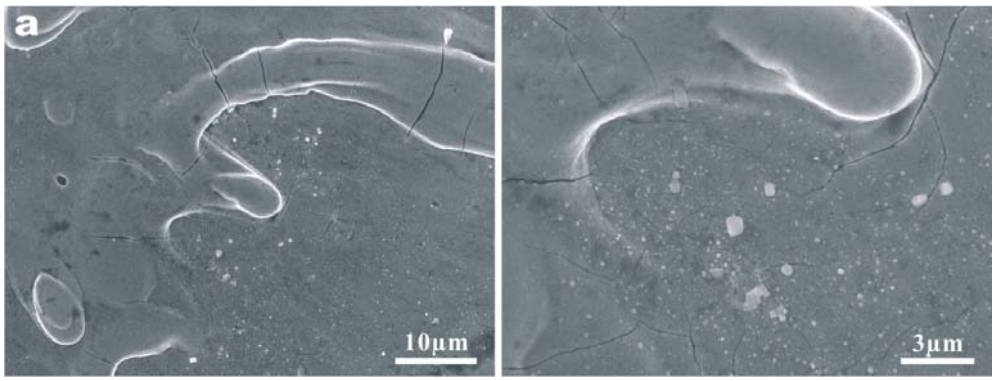

(a) near the center of the crater

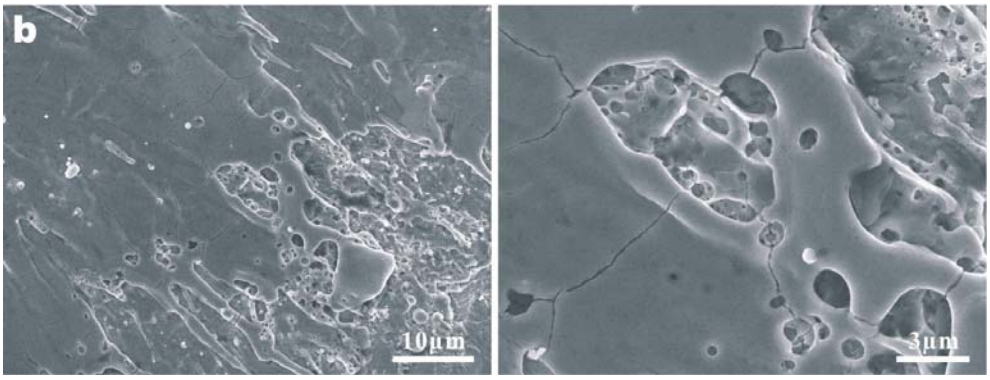

(b) between the crater center and HAZ

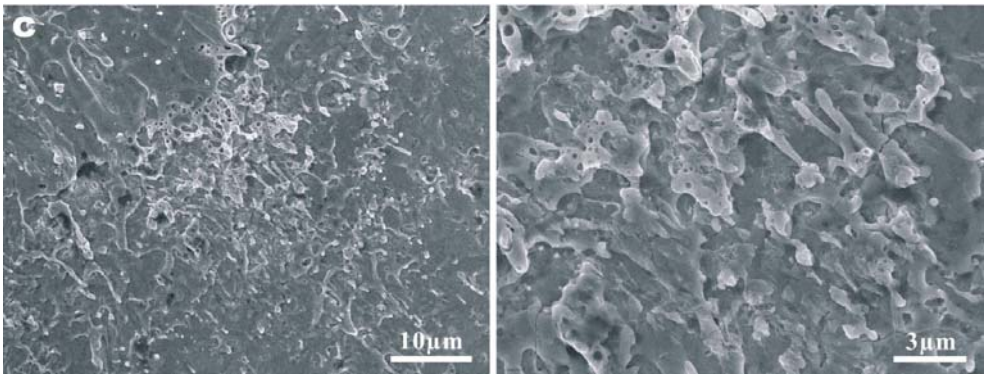

(c) within the HAZ

Fig. 3 SEM secondary electron images in low (left) and high magnification (right) showing top view of the laser ablated α-titanium plate from three areas with progressively lesser extent of melting, cracking and porosity. PLA at 520 mJ/pulse in water using single-shot Q-switch mode.

2. TEM observations of the residual stress of α-Ti and the phase identity of oxides

The same specimen as Fig. 3 was cross-sectioned by FIB for TEM observations of the residual stress of α-Ti and the phase identity of oxides based on SAED pattern and corresponding BFI as shown in Fig. 4. Four sections designated as region A (near the center of the crater), region B (between the crater center and HAZ), region C (HAZ) and region D (between HAZ and intact area) were compared in such a TEM study. The α-titanium turned out to be predominant in all regions and minor Ti_6O with characteristic diffractions was found in region B.

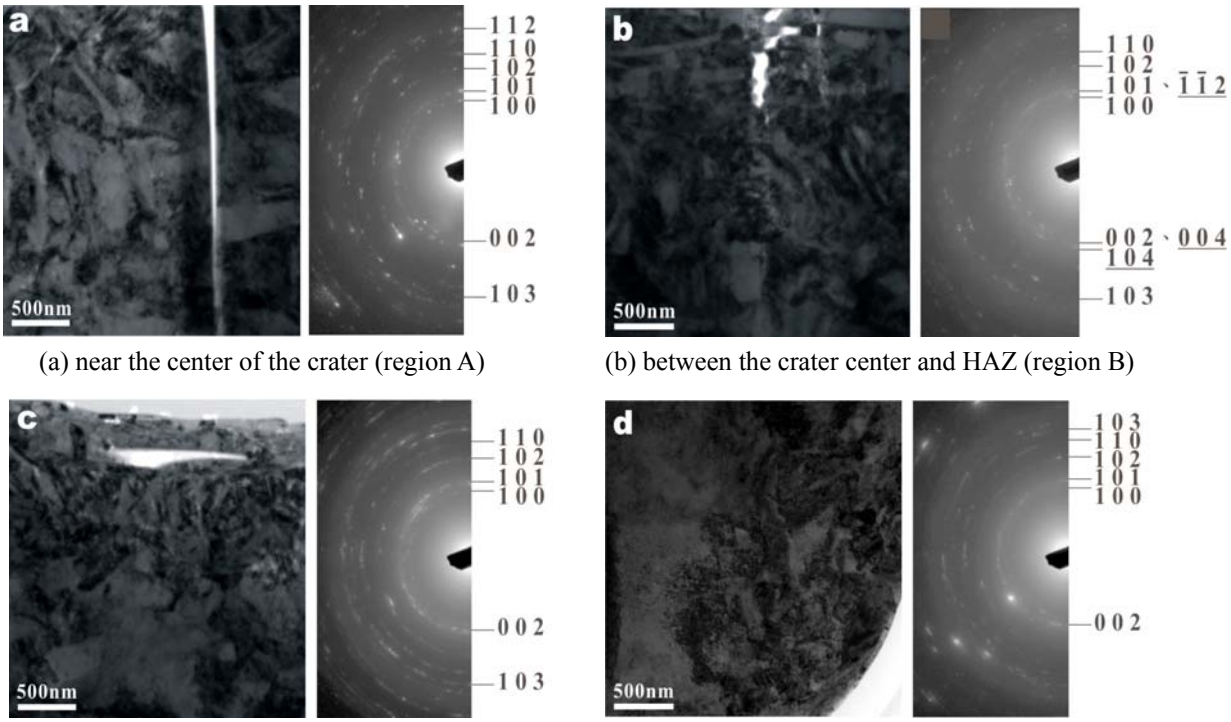

(a) near the center of the crater (region A) (b) between the crater center and HAZ (region B)

(c) within HAZ (region C) (d) between HAZ and intact area (region D)

Fig. 4 TEM BFIs and corresponding SAED patterns of the same specimen as in Fig. 3 but cross sectioned by FIB from specific areas having laser incidence side on the top of each photo.

The SAED patterns of α-Ti taken from the upper level 1 and lower level 2 of the cross section in the four areas were used for least-squares refinement of the measured d-spacings (as compiled in Table 2) and hence the cell volume, regarding the possible residual stress (as compiled in Table 3) based on the known equation of state (EOS) [10]. The resultant stress distribution along the cross section A to D as marked on the corresponding SEM image in Fig. 5 indicated that the upper level 1 has a higher residual stress than lower level 2 and region C has the highest residual stress.

Table 2 Observed d-spacings of α-Ti, based on SAED patterns from the cross section of laser ablated regions A to D in Figs. 4 and 5. The subscripts 1 and 2 denote upper and lower level, respectively of the bombarded section

hkl/region	JCPDS #44-1294	A1	A2	B1	B2	C1	C2	D1	D2
100	2.555	2.531	2.518	2.515	2.489	2.466	2.465	2.549	2.506
002	2.341	2.333	2.302	2.343	2.352	2.267	2.240	2.339	2.326
101	2.243	2.219	2.203	2.195	2.176	2.162	2.152	2.225	2.197
102	1.726	1.718	1.701	1.688	1.672	1.667	1.659	1.713	1.685
110	1.475	1.467	1.454	1.447	1.434	1.431	1.428	1.464	1.441
103	1.332	1.326	1.318	1.313	1.298	1.285	1.284	1.342	1.307

Table 3 Cell parameters and residual stress of α-Ti in specified regions

region/value	***a*** (nm)	***c*** (nm)	V (nm^3)	c/a	residual stress* (GPa)
A1	0.2923±0.0007	0.4666±0.0009	0.034517	1.596	2.751
A2	0.2903±0.0006	0.4610±0.0009	0.033646	1.588	6.174
B1	0.2873±0.0015	0.4669±0.0022	0.033364	1.625	7.378
B2	0.2837±0.0026	0.4674±0.0037	0.032590	1.648	10.932
C1	0.2849±0.0006	0.4529±0.0009	0.031830	1.590	14.825
C2	0.2845±0.0008	0.4483±0.0011	0.031415	1.576	17.138
D1	0.2923±0.0011	0.4683±0.0016	0.034641	1.602	2.256
D2	0.2874±0.0012	0.4639±0.0017	0.033182	1.614	8.179

* based on Birch-Murnagham equation of state with V_o = 35.302 $Å^3$, B_o = 117 GPa, B_o' = 3.9 GPa (cf. text)

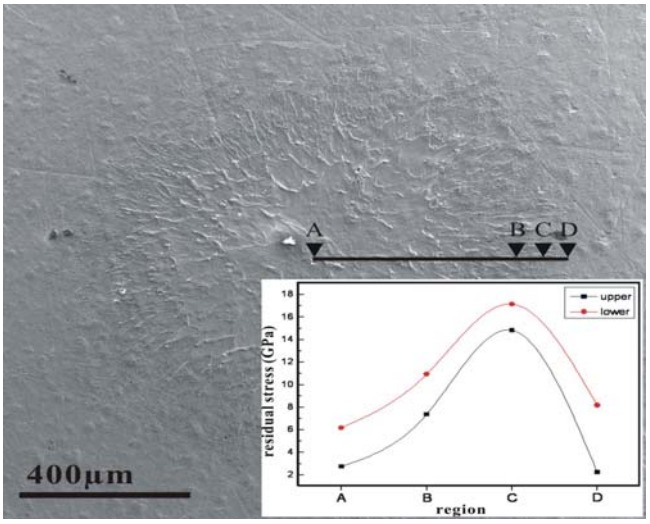

Fig. 5 SEM secondary electron image showing the whole PLA area of the α-Ti plate in Fig. 3 with regions A (near the crater center), B, C, and D (in HAZ) cross sectioned by FIB for TEM imaging and electron diffraction study in Fig. 5.

TEM BFI of the specimen sliced from region B shows a submicron-sized particle with an irregular shape (Fig. 6a). The corresponding SAED pattern (Fig. 6b) and point-count EDX spectrum (Fig. 6c) indicated that the particle is Ti_6O (space group $P\bar{3}1c$, JCPDS#72-1807) in [541] zone axis with strong Ti and rather weak O peaks.

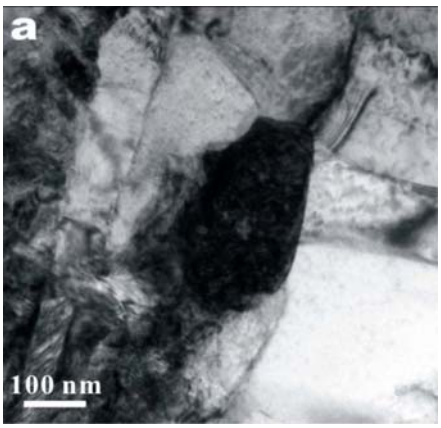

(a) TEM BFI

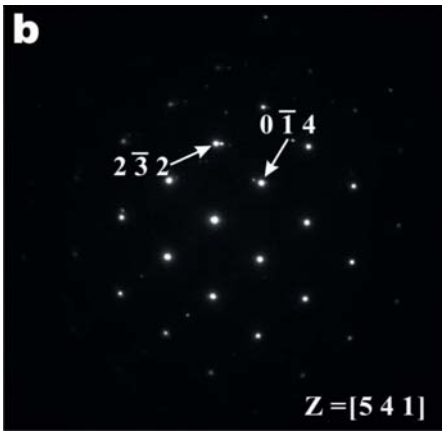

(b) SAED pattern

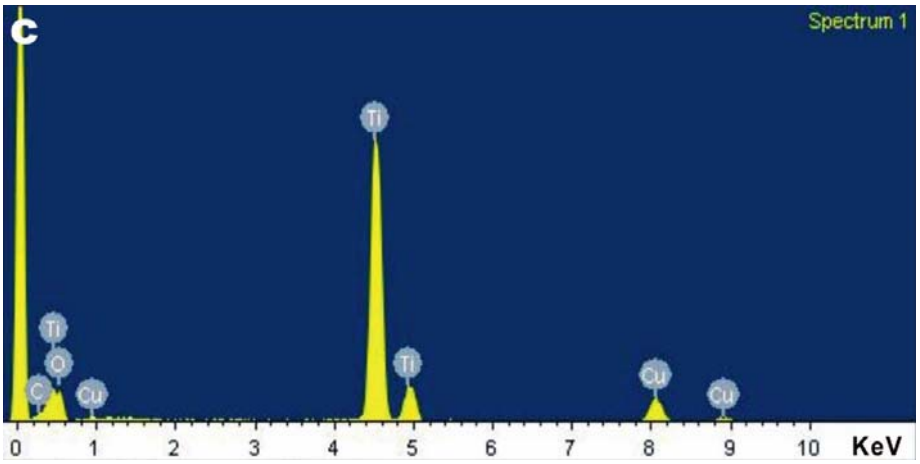

(c) Point-count EDX spectrum

Fig. 6 TEM BFI, SAED pattern and point-count EDX spectrum of the specimen sliced from region B in Fig. 4 showing irregular-shaped Ti_6O particle with Bragg diffraction contrast in [541] zone axis.

The Ti_6O particle with columnar shape was also observed (Fig. 7). The well developed surface of this particle appeared to be a pseudomorph of a precursor phase, presumably an α-Ti grain. Submicron-sized oxide of other stoichiometry and crystal structure, such as Ti_3O (space group $P\bar{3}1c$, JCPDS#72-1806) was also revealed by TEM BFI coupled with SAED pattern and point-count EDX analysis (Fig. 8).

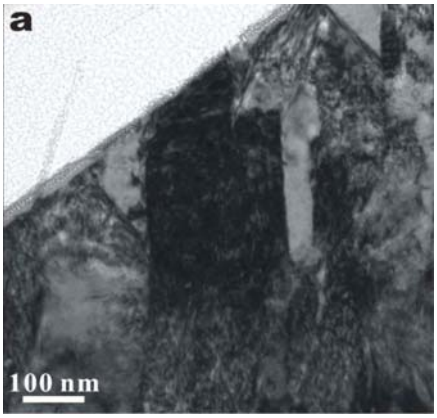

(a) TEM BFI

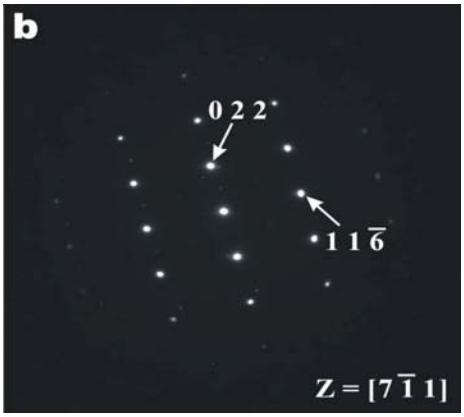

(b) SAED pattern

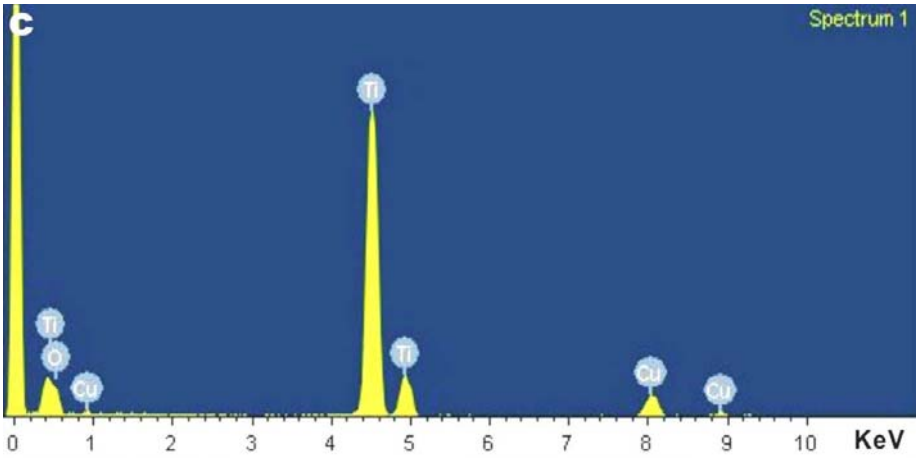

(c) Point-count EDX spectrum

Fig. 7 TEM BFI, SAED pattern and point-count EDX spectrum of the specimen sliced from region B in Fig. 4 showing columnar Ti_6O phase with Bragg diffraction contrast in [7$\bar{1}$1] zone axis

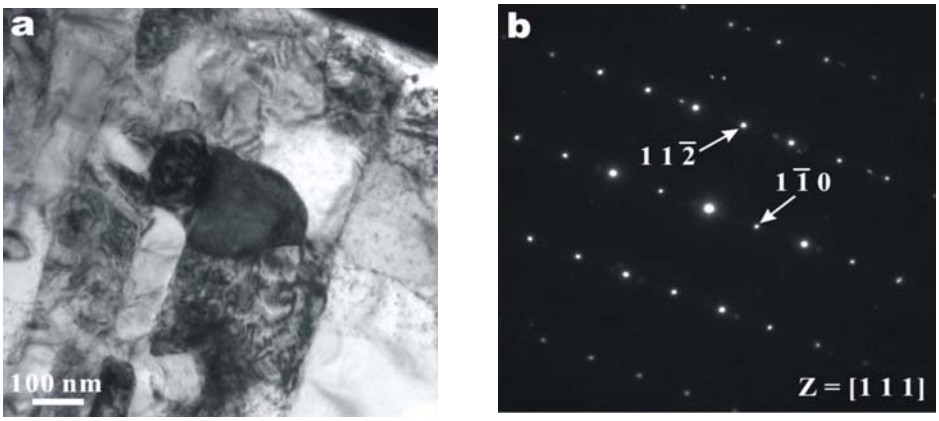

(a) TEM BFI (b) SAED pattern

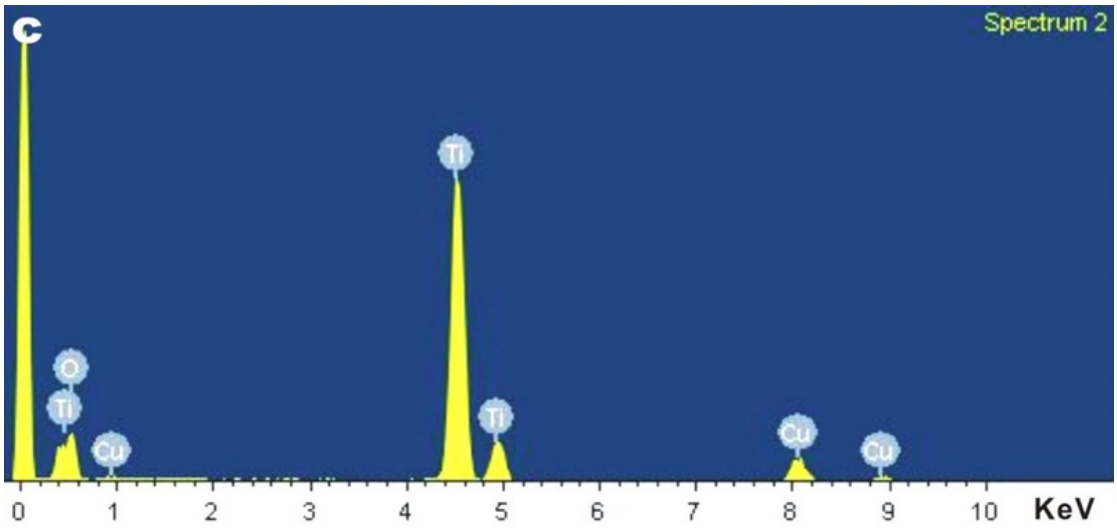

(c) Point-count EDX spectrum

Fig. 8 TEM BFI, SAED pattern and point-count EDX spectrum of the specimen sliced from region B in Fig. 4 showing Ti_3O grain in [111] zone axis with extra diffractions from neighboring grains.

IV. Discussion

1. Environmental dependence of crater diameter and HAZ width

In general, a less HAZ associated with a less extent of grain coarsening, precipitation and impurity segregation is preferred for the welded materials [11]. The crater diameter was found to decrease whereas HAZ width increases in the order of water, air and vacuum environment when laser under the same focal length and power density was introduced to the Ti plate target. The smallest crater diameter is associated with a central drill hole and the widest HAZ for the Ti plate subjected to PLA in vacuum. This can be rationalized by the least loss of input energy (i.e. least beam broadening) and the poorest heat dissipation in vacuum than other environments. In comparison with air, water environment has a more significant beam broadening effect to form a larger crater diameter, and a more effective heat dissipation to form a less HAZ on the Ti plate when subjected to PLA.

As for the effect of power density on crater and HAZ dimension, it was concluded that higher pulse energy causes a slight increase of crater diameter when produced in air and water, but no significant change when

produced in vacuum (Fig. 2a). This indicates that the limited extent of beam broadening is rather inert for the case of PLA in vacuum. On the other hand, a relatively high pulse energy caused a significant increase of HAZ width when produced in vacuum and air but not in water (Fig. 2b), in accordance with the most effective heat dissipation through water. Three characteristic time scales concerning the plasma generation and retention during thermal confinement in a dynamic process such as PLA are τ_e (the electron cooling time) which is in the order of 1 ps; τ_l (the lattice heating time); and τ_p (the duration of laser pulse) [3]. Note τ_e and τ_l are proportional to their heat capacity divided by a same constant, and the heat capacity of electron is much less than that of lattice, so $\tau_e << \tau_l$, where τ_e, τ_l are decided by materials whereas τ_p is what one can readily choose to make a difference in a PLA process.

In general, τ_p falls in ns, picosecond (ps) and fs regimes depending on how harsh the laser parameters are adopted. For the present Q-switched laser, τ_p is of ns regime and τ_p >1 ns >> τ_l >> τ_e. Under such a condition, the electrons with absorbed laser energy have enough time to be transferred to the lattice for thermal equilibrium or so called thermal confinement [12-14], and the main energy loss is the heat conduction into the solid target. (τ_p is typically shorter than the time of dissipation of the absorbed laser energy by the thermal conduction, and this condition is commonly referred to as thermal confinement.[12-14]) As a result, the target material can be over heated much beyond the melting temperature. An onset of massive material removal or ablation, is defined in this case by the critical energy density sufficient for the overheating of the surface layer up to the limit of its thermodynamic stability.

The phase explosion during PLA would cause a spontaneous decomposition of the ejected plume into a two-phase system, i.e. high-pressure high-temperature laser induced plasma (LIP) and liquid droplets in view of thermodynamic considerations [14] and experimental results [3]. Thermodynamic prediction also suggests that the LIP would generate a recoil pressure on the target [15]. In general, the piston mechanism [16] of melt ejection by the recoil pressure and an overheated substrate account for the solidification layer and HAZ near the crater by laser ablation [3]. For melting-free ablation to be possible, two conditions must be met, ultra-short pulse duration (such as fs) and high enough pulse energy.

The LIP duration, i.e. the plasma relaxation time, generated by the present ns pulsed laser is expected to be 10 times shorter for PLA in liquid than in air [17]. Besides, the maximum diameter of LIP expansion is 3 times shorter for PLA in liquid than in air [17]. Thus, PLA in water rather than air would reduce the HAZ of laser-irradiated Ti plate, as observed in this study.

2. Residual stress and recrystallization/oxidation of α–Ti plate upon PLAL

A metal target subjected to PLAL is expected to suffer a considerable residual stress because of the drastic temperature and pressure changes of the target as well as liquid under the influence of shock wave in such a dynamic process. It is commonly accepted that the laser-induced plasma expands adiabatically at a supersonic velocity creating a shock wave of high temperature/pressure/density in the plasma plume under the confinement of liquid [15]. In general, the plasma-induced pressure depends on the laser parameters, in particular the wavelength and power of the laser pulse. (For instance, PLAL of Al in water under 308 nm XeCl excimer laser with a specified pulse duration (50 ns) and laser power (1-2 GW/cm^2) was shown to reach a pressure level as high as 2-2.5 GPa in the laser-induced plasma. [18]) The liquid-solid interface where the laser pulse irradiated would tend to form a surface coating with high residual stress and even metastable phases when quenched from high temperature and high pressure [19]. This accounts for a higher residual stress in the upper level of the target plate as shown by the stress profile across the sections by FIB (Fig. 5). The residual stress is higher in HAZ (i.e. region C in Fig. 5) rather than the crater center with melting texture characteristic of a solidification

process. This can be attributed to anisotropic thermal expansion and heat conductivity of the Ti target plate more or less recrystallized and oxidized during the dynamic process.

In comparison with the original microstructure (not shown), the α-Ti plate subjected to PLA in water showed recrystallized texture and oxides, in particular in the region near HAZ, as a result of residual stress relief and high temperature oxidation, respectively. Metal oxidation is a multi-sequence process, i.e. transport of the oxide molecules to the oxide/gas interface, adsorption, dissociation, transport of the species (oxide and metal ions, electrons and holes) to the reaction site through the oxide layer, the chemical reaction itself, etc [20]. High temperature oxidation in the present dynamic process of PLAL is expected to be even more complicated. Apparently, oxygen supply from turbulent water bubbles or water itself would react with the ablated Ti surface near HAZ to form Ti_6O and Ti_3O (having oxygen ordering in the hexagonal α-Ti structure [21]) with round shape or platy like as a pseudomorph of α-Ti. Such a high-temperature oxidation is in accord with the Ti-O phase diagram [22] and previous experimental results of PLA on titanium substrate [23].

3. Engineering implications

This study shows that the crater diameter decreases whereas HAZ width increases in the order of water, air and vacuum environment when laser beam of specified pulse energy was introduced to the Ti plate target. This knowledge is in accord with a higher ablation rate of other materials by PLA in a confining liquid, than vacuum and diluted gas [19], and may shed light on some engineering applications as following.

A liquid layer is beneficial in the reduction of ablation threshold and the enhancement of ablation yields [24] for more effective films deposition and small particles synthesis [19]. In the latter aspect, experimental results and theoretical analysis, the HPHT plasma and the short quenching times, indicate that laser ablation of a solid target in a confining liquid provides an effective means to synthesize nanocrystals, especially for the metastable nanocrystals such as diamond and carbon related materials, immiscible alloys, etc. These advantages allow one to combine selected solid targets and liquid to fabricate compound nanostructures with desired functions [19].

The other potential applications are liquid-assisted materials processing including surface patterning, surface cleaning, surface coating, etching, cutting, and shock processing as suggested for various materials [1,2]. In the case of water-assisted such materials processing, in particular that involving water containing materials such as biological tissues, it is desirable that water does not absorb much laser energy following the Beer Lambert law $I_x=I_o\exp(-x/\triangle)$, where I_o is the entrance laser intensity and I_x the laser intensity in water, x the traveling distance and △ light absorption length. In fact, water was reported to be most transparent in green light region using copper vapor laser and second harmonic Nd:YAG laser with a wavelength of 511 and 532 nm, respectively [1]. Further PLA in water using a second harmonic rather than a full UV wavelength (1064 nm) of Nd:YAG laser is therefore of great interest to study the possible microstructural and phase changes on the ablated Ti plate for potential applications on aerospace, submarine and biological materials processing.

V. Conclusions

Polycrystalline α-Ti plates subjected to pulse laser ablation in a single pulse of specified energies showed power density and environment dependences of crater and HAZ dimensions. The crater diameter decreases whereas HAZ width increases in the order of water, air and vacuum environment under the same laser focal length and power density. Besides, a higher power density causes a significant increase of crater diameter for PLA in air and water but not vacuum with the least beam broadening effect. The increase of HAZ width with power density is significant for PLA in vacuum and air but not in water due to its effective heat dissipation.

According to electron diffraction measurements and Birch-Murnagham equation of state, the residual stress of the α-Ti subjected to PLA in water was estimated to be up to ca. 17 GPa in the upper level of the HAZ which showed solidified/recrystallized textures and submicron-sized Ti_6O and Ti_3O particles due to high temperature oxidation in the dynamic PLA process.

References

[1] A. Kruusing. (2004). Underwater and water-assisted laser processing: Part 1—general features, steam cleaning and shock processing, *Optics and Lasers in Engineering, 41*(2), 307-327.

[2] A. Kruusing. (2004). Underwater and water-assisted laser processing: Part 2—Etching, cutting and rarely used methods, *Optics and Lasers in Engineering, 41*(2), 329-352.

[3] B. N. Chichkov, C. Momma, S. Nolte, F. von Alvensleben, and A. Tünnermann. (1996). Femtosecond, picosecond and nanosecond laser ablation of solids, *Appl. Phys. A, 63*(2), 109-115.

[4] C. Momma, B. N. Chichkov, S. Nolte, F. von Alvensleben, A. Tünnermann, H. Welling, and B. Wellegehausen. (1996). Short-pulse laser ablation of solid targets, *Optics Comm., 129*(1-2), 134-142.

[5] R. Le Harzic, N. Huot, E. Audouard, C. Jonin, P. Laport, S. Valette, A. Fraczkiewicz, and R. Fortunier. (2002). Comparison of heat-affected zones due to nanosecond and femtosecond laser pulses using transmission electronic microscopy, *Appl. Phys. Lett.,* 80, 3886-3888.

[6] S. Y. Chen, and P. Shen. (2002). Laser Ablation Condensation of α−PbO_2-Type TiO_2, *Phys. Rev. Lett., 89*, 096106-1.

[7] S. Y. Chen, and P. Shen. (2004). Laser Ablation Condensation and Transformation of Baddeleyite-Type Related TiO_2, *Jpn. J. Appl. Phys., 43*(4A), 1519-1524.

[8] A. Salleo, S. T. Taylor, M. C. Martin, W. R. Panero, R. Jeanloz, T. Sands, and F. Y. Genin. (2003). Laser-driven formation of a high-pressure phase in amorphous silica, *Nature Materials, 2*, 796-800.

[9] D. B. Williams. (1984). *Practical Analytical Electron Microscopy in Materials Science*, Philips Electronic Instruments, Inc.: New Jercy.

[10] D. Errando, Y. Meng, M. Somayazulu, and D. Hausermann. (2005). D. Errando, Y. Meng, M. Somayazulu, and D. Hausermann. (2005). *Physica B, 355*, 116-125.

[11] J. H. Kim, Y. J . Oh, I. S. Hwang, D. J. Kim, and J. T. Kim. (2001). Fracture behavior of heat-affected zone in low alloy steels, *J. Nuclear Mater., 299*(2), 132-139.

[12] S. L. Jacques. (1993). Role of tissue optics and pulse duration on tissue effects during high-power laser irradiation, *Appl. Opt., 32*(13), 2447-2454. (doi: 10.1364/AO.32.002447)

[13] L. V. Zhigilei and B. J. Garrison. (1999). Molecular dynamics simulation study of the fluence dependence of particle yield and plume composition in laser desorption and ablation of organic solids, *Appl. Phys. Lett., 74*, 1341-1343.

[14] L. V. Zhigilei and B. J. Garrison. (2000). Microscopic mechanisms of laser ablation of organic solids in the thermal and stress confinement irradiation regimes, *J. Appl. Phys.,* 88, 1281-1298.

[15] R. Fabbro, J. Fournier, P. Ballard, D. Devaux, and J. Virmont. (1990). Physical study of laser-produced

plasma in confined geometry, *J. Appl. Phys.,* 68, 775-784.

[16] M. Von Allmen and A. Blatter. (1994). *Laser-Beam Interactions with Materials*, Springer: New York.

[17] K. Saito, K. Takatani, T. Sakka, and Y. H. Ogata. (2002). Observation of the light emitting region produced by pulsed laser irradiation to a solid–liquid interface, *Appl. Surf. Sci.,* 197, 56-60.

[18] L. Berthe, A. Sollier, R. Fabbro, P. Peyer, and E. Bartnicki. (2000). The generation of laser shock waves in a water-confinement regime with 50 ns and 150 ns XeCl excimer laser pulses, *J. Phys. D,* 33, 2142-2145.

[19] G. W. Yang. (2007). Laser ablation in liquids: Applications in the synthesis of nanocrystals, *Prog. Mater. Sci.,* 52, 648-698.

[20] L. Nanai, R. Vajtai, and T. F. George. (1997). Laser-induced oxidation of metals: state of the art, *Thin Solid Films, 298*(1-2), 160-164.

[21] M. L. Wasz, F. R. Brotzen, R. B. McLellan, and A.J. Griffin. (1996). Effect of oxygen and hydrogen on mechanical properties of commercial purity titanium, *Int. Mater. Rev., 41*(1), 1-12.

[22] P. Waldner and G. Eriksson. (1999). Thermodynamic modelling of the system titanium-oxygen, *Calphad, 23*(2), 189-218.

[23] L. Lavisse, D. Grevey, C. Langlade, and B. Vannes. (2002). The early stage of the laser-induced oxidation of titanium substrates, *Appl. Surf. Sci., 186*(1-4), 150-155.

[24] D. S. Kim, B. OH, and H. Lee. (2004). Effect of liquid film on near-threshold laser ablation of a solid surface, *Appl. Surf. Sci., 222*(1-4), 138-147.